

Molecular hydrogen from $z = 0.0963$ DLA Towards the QSO J1619+3342^{*}

R. Srianand¹†, H. Rahmani^{1,2}, S. Muzahid³ and V. Mohan¹

¹ Inter-University Centre for Astronomy and Astrophysics, Post Bag 4, Ganeshkhind, Pune 411 007, India

² School of Astronomy, Institute for Research in Fundamental Sciences (IPM), PO Box 19395-5531, Tehran, Iran

³ The Pennsylvania State University, 413 Davey Lab, University Park, State College, PA 16802, USA

7 June 2021

ABSTRACT

We report the detection of H_2 in a $z_{\text{abs}} = 0.0963$ Damped Lyman- α (DLA) system towards $z_{\text{em}} = 0.4716$ QSO J1619+3342. This DLA has $\log N(\text{H I}) = 20.55 \pm 0.10$, $18.13 \leq \log N(\text{H}_2) \leq 18.40$, $[\text{S}/\text{H}] = -0.62 \pm 0.13$, $[\text{Fe}/\text{S}] = -1.00 \pm 0.17$ and the molecular fraction $-2.11 \leq \log[f(\text{H}_2)] \leq -1.85$. The inferred gas kinetic temperature using the rotational level population is in the range 95–132 K. We do not detect C I or C II* absorption from this system. Using R and V band deep images we identify a sub- L_* galaxy at an impact parameter of 14 kpc from the line of sight, having consistent photometric redshift, as a possible host for the absorber. We use the photoionization code `CLOUDY` to get the physical conditions in the H_2 component using the observational constraints from H_2 , C I, C II* and Mg I. All the observations can be consistently explained if one or more of the following is true: (i) Carbon is underabundant by more than 0.6 dex as seen in halo stars with $Z \sim 0.1 Z_\odot$, (ii) H I associated with H_2 component is less than 50% of the H I measured along the line of sight and (iii) the H_2 formation rate on the dust grains is at least a factor two higher than what is typically used in analytic calculations for Milky Way interstellar medium. Even when these are satisfied, the gas kinetic temperature in the models are much lower than what is inferred from the ortho-para ratio of the molecular hydrogen. Alternatively the high kinetic temperature could be a consequence of contribution to the gas heating from non-radiative heating processes seen in hydrodynamical simulations.

Key words: galaxies: quasar: absorption line – galaxies: ISM – quasar: individual: J1619+3342

1 INTRODUCTION

Damped Lyman- α systems (DLAs) are the highest H I column density absorbers seen in QSO spectra, with $N(\text{H I}) \geq 2 \times 10^{20} \text{ cm}^{-2}$ (see Wolfe et al. 2005, for a review). These absorbers trace bulk of the neutral hydrogen at $2 < z < 3$ (Prochaska et al. 2005; Noterdaeme et al. 2009b, 2012) and have been conjectured to be originating from the gas associated with high- z galaxies and proto-galaxies. The link between DLAs and galaxies can be established by directly detecting galaxies and/or showing that the prevailing physical conditions in the absorbing gas are consistent with those seen in a typical galactic Interstellar Medium (ISM).

Our understanding of the physical conditions in DLAs is primarily based on optical absorption-line studies, involving the detec-

tion of low-ionization metal transitions and, in a few cases, H_2 , HD and CO molecular absorption (see for example, Ledoux et al. 2003; Srianand et al. 2008; Varshalovich et al. 2001; Noterdaeme et al. 2008a,b, 2009a). DLA subcomponents in which H_2 absorption is detected, have typical temperature and density of $153 \pm 78 \text{ K}$ and $n_{\text{H}} = 10\text{--}200 \text{ cm}^{-3}$, respectively (Srianand et al. 2005). The gas producing H_2 absorption probably traces diffuse molecular gas that is compact (Balashev et al. 2011) containing only a small fraction of H I measured using the DLA profile (Srianand et al. 2012). When CO is detected one gets a chance to probe high- z translucent regions (Noterdaeme et al. 2010a) and rotational excitations of CO are mainly dominated by the pumping by cosmic microwave background (Srianand et al. 2008; Noterdaeme et al. 2011). The C II* absorption, detected in roughly 50% of the high- z DLAs, is also used to infer physical conditions (Wolfe et al. 2008). The inferred radiation field, using some of these indicators when present, is similar to the mean Galactic field probably originating from local star formation activities. However, direct detection of host galaxies of these high- z DLAs is needed to firmly establish a direct link be-

* Based on observations made with the NASA/ESA Hubble Space Telescope, obtained from the data archive at the Space Telescope Science Institute, which is operated by the Association of Universities for Research in Astronomy, Inc., under NASA contract NAS 5-26555.
† email: anand@iucaa.ernet.in

tween galaxy properties and the physical conditions inferred using various indicators discussed here.

Despite several attempts a firm link between galaxies and DLAs is not established at high- z , mainly due to the paucity of direct detection of galaxies. Only few DLAs with high metallicity and high $N(\text{H I})$ are detected through the Lyman- α emission (see Fynbo et al. 2013, and references there for the summary). Observed host galaxies are usually found at large impact parameters suggesting that the absorbing gas is located well outside the luminous part of the galaxy and large-scale winds and outflows are playing a vital role in populating the circumgalactic regions of these high- z galaxies with cold gas (Bouché et al. 2013; Fynbo et al. 2013; Kashikawa et al. 2014). Such a picture is also supported by simulations (see Pontzen et al. 2008; Altay et al. 2011). However, host galaxies are not detected for most of the DLAs that show H_2 and/or C II^* at high- z .

At low- z (i.e., $z \leq 1$) it is relatively easy to identify the galaxy counterparts of DLAs and sub-DLAs (Burbidge et al. 1996; Le Brun et al. 1997; Rao et al. 2003; Meiring et al. 2011; Battisti et al. 2012). Associated galaxies span a wide range of morphology and impact parameters. Establishing the connection between physical conditions derived from above mentioned indicators and the star formation activities in low- z galaxies will enable us to interpret the high- z DLA observations. However, only a few low- z DLAs are known (see for example, Rao et al. 2006) and only two H_2 detections are known at $z \leq 1$ (Crighton et al. 2013; Oliveira et al. 2014). Thanks to HST/COS the situation is improving rapidly (Meiring et al. 2011; Battisti et al. 2012). Here we present the detection of H_2 in a $z_{\text{abs}} = 0.0963$ DLA towards the QSO J1619+3342 and study the physical conditions prevailing in this system.

2 OBSERVATIONS AND DATA REDUCTION

The ultraviolet (UV) spectrum of the QSO SDSS J161916.54+334238.4 ($z_{\text{em}} \sim 0.4716$; refer to as J1619+3342 in this paper) was obtained using the Cosmic Origins Spectrograph (COS) on board the *Hubble Space Telescope* (HST) during observing cycle-17, under program ID: 11598 (PI: Jason Tumlinson). The observations consist of G130M (5.3 ks) and G160M (8.8 ks) far-UV (FUV) grating integrations at a medium resolution of $R \sim 18,000$ (FWHM $\sim 18 \text{ km s}^{-1}$). The data were retrieved from the HST archive and reduced using the STScI CALCOS (v2.17.3) pipeline software. The individual reduced *x1d* files were flux calibrated. The alignment and co-addition of the separate G130M and G160M exposures were done using the software developed by Danforth et al. (2010)¹. The exposures were weighted by the integration time while co-adding the flux calibrated data. The final coadded spectrum covers the wavelength range 1134 – 1796 Å with the signal-to-noise ratio $S/N \sim 8$ –12 per resolution element. Each COS resolution element is sampled by six raw pixels. We therefore binned the spectrum by 3 pixels and perform most of our analysis/measurements using this binned data. Continuum normalization was done by fitting the line free regions with a smooth lower order polynomial.

The COS wavelength calibration known to have uncertainties at the level of 10–15 km s^{-1} . Regions of spectrum that are recorded near the edges of the detector segment are more prone to have such

erroneous wavelength solution (Savage et al. 2011; Meiring et al. 2013). It is also known that the line spread function (LSF) of the COS spectrograph is not a Gaussian. A characterization of the non-Gaussian COS LSF is found in Ghavamian et al. (2009) and subsequently updated by Kriss (2011). We adopt the Kriss (2011) LSF for our Voigt profile fitting analysis. Interpolated LSF at the line center were convolved with the model Voigt profile while fitting an absorption line using the *vpfit*² code.

We used the 2-m telescope at IUCAA Girawali Observatory (IGO) to image the field in R and V bands using IUCAA Faint Object Spectrograph and Camera (IFOSC) on 20-21 March 2013. Total exposure times are 3900s and 4900s in V and R band respectively. A typical seeing during these observations was in the range 1.3 to 1.4 arcsec. However, as these images are much deeper than those of SDSS, we use them to identify nearby galaxies to the QSO line of sight.

3 PROPERTIES OF THE DLA FROM THE ABSORPTION LINE ANALYSIS

3.1 Measurements based on atomic lines

In this sub-section we derive physical conditions using the metal line absorption originating from neutral and singly ionized species.

3.1.1 Metallicity and dust depletion

Column density and metallicity measurements for this DLA are presented in detail in Table 3 of Battisti et al. (2012). These authors find $\log N(\text{H I}) = 20.55 \pm 0.10$, $[\text{S}/\text{H}] = -0.62 \pm 0.13$, $[\text{N}/\text{H}] = -1.74 \pm 0.16^3$, $[\text{P}/\text{H}] = -0.81 \pm 0.21$ and $[\text{Fe}/\text{S}] = -1.00 \pm 0.17$. In addition to these, we measure $\log N(\text{Ar I}) = 14.12 \pm 0.11$ and obtain 3σ upper limits⁴: $\log N(\text{Cl I}) \leq 13.09$, $\log N(\text{C I}) \leq 13.30$ and $\log N(\text{C II}^*) \leq 13.12$ (Battisti et al. 2012) using the COS spectrum. Based on Ar I, which is the dominant ionization stage of Ar in the neutral gas, we get $[\text{Ar}/\text{H}] = -0.83 \pm 0.16$. Note $[\text{Ar}/\text{S}] = -0.21 \pm 0.14$ also confirms that the Ar is mostly in Ar I if we assume that the intrinsic $[\text{Ar}/\text{S}]$ is solar. This suggests that the gas may not be ionized by a hard radiation field (Vladilo et al. 2003). From Battisti et al. (2012) we also have $\log N(\text{Mg I}) = 12.40 \pm 0.14$, $\log N(\text{Ca II}) = 12.42 \pm 0.02$ and $\log N(\text{Ti II}) = 11.90 \pm 0.04$ based on their KECK/HIRES spectrum that also shows the metal absorption to be present in two distinct velocity components separated by $\sim 9 \text{ km s}^{-1}$. Note at the HST/COS's resolution the two components are not resolved. Therefore, we use the total column density for all the analysis presented below. The measured $[\text{Ti}/\text{S}] = -0.90 \pm 0.10$ suggests that, for the measured $N(\text{H I})$, the Ti depletion is much less than what is typically seen in the Milky Way disk and in the lower end of the measurements towards Milky Way outer halo or Large Magellanic clouds (LMC, see Fig 3 of, Welty & Crowther 2010). They also suggested that the sight lines with such values of $[\text{Ti}/\text{S}]$ may be related to gas having low density and low molecular fraction (i.e., $f(\text{H}_2) = 2N(\text{H}_2)/[N(\text{H I}) + 2N(\text{H}_2)] \leq 0.1$).

It is found that the ratio of $N(\text{Ti II})$ to $N(\text{Ca II})$ remains nearly constant in the local measurements. This ratio has a value of ~ 0.3

² <http://www.ast.cam.ac.uk/~rfc/vpfit.html>

³ Only N I column density is used to derive $[\text{N}/\text{H}]$ and we do not include contribution from N II.

⁴ Using Ar $\lambda\lambda 1048, 1066, \text{Cl } \lambda 1347, \text{C } \lambda 1650$ and $\text{C II}^* \lambda 1335$ transitions.

¹ <http://casa.colorado.edu/~danforth/science/cos/costools.html>

Table 1. Results of single cloud curve of growth for H₂ absorption

Level	Transition	λ_r (Å)	f (10 ⁻²)	λ_r (range) (Å)	W_0 (Å)	δW_0		log[N(cm ⁻²)]	
						(sta) (Å)	(sys) (Å)	COG ⁺	VPFIT
J = 0	L ₁ R ₀	1092.1952	0.578	1092.11-1092.50	0.157	0.008	0.008	17.54–17.90	18.17±0.04
	L ₂ R ₀	1077.1387	1.170	1077.06-1077.33	0.147	0.006	0.008		
	L ₄ R ₀	1049.3673	2.310	1049.23-1049.54	0.172	0.011	0.008		
J = 1	L ₁ R ₁	1092.7323	0.378	1092.65-1092.94	0.123	0.006	0.012	18.00–18.22	18.36±0.04
	L ₂ P ₁	1078.9254	0.392	1078.81-1079.14	0.164	0.008	0.012		
	L ₃ R ₁	1063.4601	1.190	1063.35-1063.70	0.189	0.007	0.012		
	L ₄ R ₁	1049.9597	1.550	1049.84-1050.16	0.193	0.010	0.009		
	L ₅ P ₁	1038.1570	0.866	1038.00-1038.30	0.171	0.012	0.010		
J = 2	L ₀ P ₂	1112.4959	0.069	1112.37-1112.70	0.048	0.007	0.025	15.44–16.88	15.97±0.25
	L ₁ P ₂	1096.4383	0.236	1096.34-1096.60	0.070	0.007	0.013		
	L ₂ P ₂	1081.2659	0.469	1081.21-1081.42	0.057	0.009	0.010		
	L ₂ R ₂	1079.2254	0.681	1079.14-1079.36	0.075	0.007	0.010		
	L ₃ P ₂	1066.9006	0.709	1066.84-1067.05	0.083	0.007	0.010		
	L ₃ R ₂	1064.9947	1.060	1064.92-1065.19	0.083	0.008	0.013		
	L ₄ P ₂	1053.2842	0.902	1053.14-1053.44	0.094	0.010	0.015		
	L ₅ P ₂	1040.3672	1.020	1040.20-1040.47	0.095	0.013	0.012		
	L ₅ R ₂	1038.6901	1.660	1038.59-1038.77	0.072	0.011	0.008		
	J=3	L ₄ R ₃	1053.9760	1.340	1053.80-1054.15	0.072	0.010		
L ₅ R ₃		1041.1588	1.580	1041.05-1041.22	0.048	0.010	0.010		

⁺ 1 σ range in column density obtained using 1 σ range in b and W_0 .

in the Galactic ISM and ~ 0.9 in the case of LMC and Small Magellanic Clouds (SMC, see Cox et al. 2006, 2007). It is interesting to note that in the present case we find this ratio to be 0.3 consistent with the Milky Way measurements. We also notice that the ratio of $N(\text{Fe II})$ to $N(\text{Ti II})$ is close to solar suggesting similar depletion for Fe and Ti and the absence of major ionization effects. In summary, purely based on metallicity measurements we can conclude that the average metallicity [i.e., $[\text{S}/\text{H}] \sim -0.62$] is similar to the mean value measured for SMC sight lines. The depletion pattern is intermediate between lower Milky way halo gas and LMC sight lines. If the strong correlation seen between average line of sight density and Ti depletion is applicable then the gas density in the present DLA may be lower than that typically seen in the Milky Way disk (See Fig 2 of Welty & Crowther 2010).

All the above quoted abundance measurements are based on dominant neutral or singly ionized species without applying ionization corrections. However, discussions presented above suggest that the ratios of singly ionized species are not severely affected by ionization effects. Assuming intrinsic $[\text{Fe}/\text{S}]$ to be solar we get the column density of dust in Fe, $\log N(\text{Fe})_{\text{dust}} = 14.83$ and dust to gas ratio $\log \kappa = -0.74$. At high- z , DLAs with such high values of metallicity, κ and $N(\text{Fe})_{\text{dust}}$ tend to have detectable H₂ (Ledoux et al. 2003; Petitjean et al. 2006; Noterdaeme et al. 2008a).

3.1.2 The absence of C II* fine-structure line:

In the Galactic ISM, $[\text{C II}] 158\mu$ line emission is a dominant coolant in the neutral gas. If this is also the case in high- z DLAs then one can estimate the gas cooling rate per hydrogen atom (l_c) using $N(\text{C II}^*)$. Under steady state conditions, one can use this to infer the gas heating rate and hence the insitu starformation rate (Wolfe et al. 2003). Using the distribution of l_c in high- z DLAs Wolfe et al. (2008) have suggested the existence of two populations of C II* absorbers which they called “low-” and “high-cool” absorbers. In the present case we do not detect the C II* absorption. The 3 σ upper limit on $N(\text{C II}^*)$ corresponds to an upper limit

of $\log l_c \leq -27.03^5$. This is much lower than what is typically seen in the Milky Way disk and low, intermediate and high velocity clouds (Lehner et al. 2004). The upper limit also puts the present DLA amongst the “low-cool” population identified by Wolfe et al. (2008). Wolfe et al. (2008) have suggested that the “low-cool” population may either related to (i) Warm neutral medium (with $T \sim 8000$ K) in ionization equilibrium with the meta-galactic radiation field or (ii) metal poor compact region with continuously on-going insitu starformation. However, what is interesting to note is that the measured $[\text{S}/\text{H}]$ in the present case is much higher than that typically seen in high- z “high-” (mean $[\alpha/\text{H}] = -1.06 \pm 0.15$) and “low-cool” (mean $[\alpha/\text{H}] = -1.74 \pm 0.19$) absorbers. Therefore, if metallicity is the crucial factor that discriminates this two population the present DLA should belong to the higher end of the “high-cool” DLAs.

Next we look at the relationship between l_c and H₂ detections at high- z . At high- z , C II* is detected almost in all H₂ systems (with lower $N(\text{C II}^*)$ compared to the present limit in few cases) whenever the expected wavelength range is not contaminated by absorption lines from other intervening gas. However, we note that about 36% of the H₂ DLAs have $\log l_c \leq -27.03$. This suggests that even among H₂ detected DLAs (with signatures of low temperatures in the H₂ components) low l_c values as seen in the present case are not that uncommon.

Direct measurement of $N(\text{C II}^*)/N(\text{C II})$ is important to draw physical conditions in the gas. Unfortunately, it is difficult to measure the C II column density directly from the COS data. Firstly the C II $\lambda 1334$ line is saturated and partially blended with Ly β line from $z_{\text{abs}} = 0.4268$. Secondly the absorption component has a velocity shift of about 10 km s⁻¹ with respect to the z_{abs} defined by other metal lines. Based on the velocity off-set between the Lyman series lines of $z_{\text{abs}} = 0.4268$ we confirm that C II $\lambda 1334$ is highly saturated but not showing damping wings. The C II $\lambda 1036$ line is covered by the COS spectrum. Unfortunately this line is blended with another

⁵ l_c is defined in units of erg s⁻¹ per hydrogen atom

strong absorption line. Therefore, direct estimation of C II column density is difficult. So we use indirect estimations of $N(\text{C II})$ for discussions presented below.

If we assume that the abundance ratio $[\text{C/S}]$ is close to solar and no depletion of C into dust grains then we expect $\log N(\text{C II}) = 16.39$. This gives $\log N(\text{C II}^*)/N(\text{C II}) \leq -3.27$. We wish to note here that this inferred column density is allowed by the observed profile if we apply a necessary velocity shift to match the Ly β profile of $z_{\text{abs}} = 0.4268$ system with rest of the Lyman series lines. However, if the C enhancement in this DLA follows what one sees in intermediate and low metallicity halo stars in our Galaxy then we expect $[\text{C/O}] \sim -0.7$ for the metallicity observed in the present DLA (Akerman et al. 2004; Fabbian et al. 2009; Dutta et al. 2014). In such a case we will have $\log N(\text{C II}^*)/N(\text{C II}) \leq -2.57$. Note any depletion of C with respect to S due to dust depletion will further increase this ratio up to 0.4 dex (see for example Sofia et al. 2011).

As can be seen from the discussions given in Srianand et al. (2005), the predicted value of $\log N(\text{C II}^*)/N(\text{C II})$ is in the range -2.62 to -2.20 in the case of a typical Cold Neutral Medium (CNM) and in the range -2.65 to -3.17 in the case of a typical Warm Neutral Medium (WNM) of our Galaxy. However, for the typical abundance and dust depletion prevailing in high- z DLAs the corresponding ranges are -2.26 to -2.08 for CNM and -3.39 to -2.70 for WNM. It is clear that if the $[\text{C/S}]$ in this DLA is close to solar then the absence of C II* is consistent with the WNM solution. However, if $[\text{C/S}]$ is close to intermediate metallicity stars then the measured C II* upper limit will allow for a CNM solution. We come back to this issue later when we discuss photo-ionization models for this system.

3.1.3 The absence of C I absorption line:

Srianand et al. (2005) have suggested a possible connection between the presence of C I absorption and H₂ detection. Among H₂ detections available till date (excluding the CO systems detected through the presence of strong C I lines in SDSS spectrum, see Srianand et al. 2008; Noterdaeme et al. 2010a, 2011) we notice that about 73% of the high- z H₂ systems have detectable C I lines. Note most of the detected C I lines have column densities much lower than the upper limit of C I we find for the present DLA. Therefore, absence of C I absorption in the present system is not that uncommon even in high- z DLAs with H₂ detections. Following Srianand et al. (2005) we can write,

$$\frac{n_e}{\Gamma} = 4.35 \times 10^{11} \frac{N(\text{C I})}{N(\text{C II})} \left(\frac{T}{10^4} \right)^{0.64}. \quad (1)$$

We can use the observed value of $N(\text{C I})/N(\text{C II})$ to place a constraint of n_e/Γ , where Γ and n_e are the C⁰ photoionization rate and electron density respectively. When we assume $T = 100$ K [as inferred in the next session], we get $n_e/\Gamma \leq 1.8 \times 10^7$ s cm⁻³ and $n_e/\Gamma \leq 9.0 \times 10^7$ s cm⁻³ respectively for $N(\text{C II})$ obtained using $[\text{S/C}]$ close to solar and $[\text{S/C}]$ close to what is seen in intermediate metallicity halo stars. When we use the mean n_e measured by Welty et al. (2003) and Γ from Pequignot & Aldrovandi (1986) we get the mean $n_e/\Gamma \sim 7 \times 10^8$ s cm⁻³ for the diffuse interstellar medium in Milky Way. Therefore, either the absorber has larger ionization rate or has lower n_e compared to what is typically seen in CNM of our Galaxy. However, if we use $\Gamma = 2 \times 10^{-10}$ s⁻¹ (a typical value for the Milky Way ISM) then we get $n_e \leq 0.004$ and 0.012 cm⁻³ respectively for the two inferred values of $N(\text{C II})$. These are

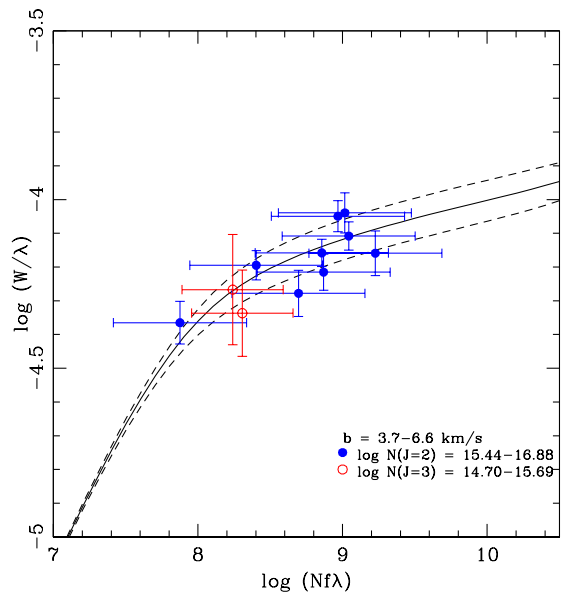


Figure 1. Results of single component curve of growth analysis. The best fitted curve for the absorption from $J = 2$ and $J = 3$ levels are shown overlaid with data points. The ordinate errors are based on the measured equivalent width errors and the abscissa errors are due to column density errors from our COG analysis.

consistent with what one sees in 40% of the components in high- z DLAs with C I detections (See Table 4 of Srianand et al. 2005).

3.1.4 High ions and velocity structure in the absorbing gas:

Battisti et al. (2012) have reported the detection of N II, Si III and Fe III in their HST/COS spectrum. From their Fig. 10, it is apparent that there is no clear velocity segregation between low ion and Fe III. We also notice that the N II absorption profile very much follows that of the singly ionized species. This means that the gas we are dealing with is a multiphase medium and some fraction of the observed column density of singly ionized species may originate from N II or Fe III phase. Weak Si IV and C IV absorption are also detected in this component. A strong C IV absorption is detected at -100 km s⁻¹ with respect to the main component. No other ion is detected in this component. As in high- z DLAs this component may probably be related to outflows (Fox et al. 2007) and may not contain much of $N(\text{H I})$ measured from the DLA profile. As discussed before consistent abundance ratios inferred from singly ionized species are a good indication for the absence of strong influence from ionization effects in this phase. However, the lack of information on H I column density of this phase will hamper our attempt to model the system using photoionization equilibrium.

3.2 H₂ measurements:

Molecular hydrogen is detected in the DLA in four rotational levels (i.e., up to $J \leq 3$). We have identified a set of uncontaminated H₂ lines for the column density measurements. Details of these H₂ lines are summarized in Table 1. In this table the first 4 columns give the rotational level, species ID, rest wavelength and oscillator strength respectively. As one expects the b-parameter of the H₂ components to be smaller than the spectral resolution of COS one

has to be careful about the hidden saturation effects while measuring column densities. In addition, the apparent shifts between different absorption lines due to wavelength calibration uncertainties and non-gaussian LSF, if not taken into account properly, can lead to wrong column density estimates when one uses Voigt profile fitting codes. So we use both curve of growth (COG) and VPFIT to constrain the b parameter and measure the H₂ column densities.

3.2.1 Curve of growth analysis:

In Table 1, we summarise rest equivalent width (W_0) measurements for the clean lines and associated errors (δW_0). We estimate two sets of errors for the observed equivalent widths. These are statistical error due to uncertainties in the flux measurements ($\delta W_0(sta)$) and systematic error from the continuum placement uncertainties ($\delta W_0(sys)$). We measure the latter by using different continuum normalisations. For the COG analysis discussed below we use combined errors.

The rest wavelength range used to get the equivalent width is also given in the 5th column of Table 1. It is clear from this table that equivalent widths from a given J levels are not scaling as λf as expected for the lines in the linear portion of the curve of growth. This suggests that saturation effects are important. The $J = 2$ level has several clean transitions observed so that one can get good constraints on N and b using the single cloud curve of growth.

When we use measured rest equivalent widths and combined errors of all 9 transitions observed for the $J = 2$ level a best fit is obtained for $\log N(\text{H}_2, J = 2) = 16.16 \pm 0.72$ and $b = (5.2 \pm 1.4)$ km s⁻¹ $\chi^2_\nu = 0.69$ (see Fig. 1). The derived b -parameter is of the order of one third of the spectral resolution of HST-COS. For simplicity we assume this b -parameter range for all the J levels to measure the column densities. In general this need not be the case as b may depend on the J levels (see for example, Noterdaeme et al. 2007). For b value similar to or less than what we obtained above the $J = 0$ and $J = 1$ lines are in the damped part of the curve of growth. Using the strongest two transitions for $J = 0$ and $J = 1$ and assuming these lines are in the damped part of the COG, we estimate the range in column densities for these levels. The column density range for each J resulting from this analysis are also summarized in Table 1.

3.2.2 Voigt profile analysis

We fitted the same set of clean H₂ lines with a single component voigt profile using the VPFIT code. In these fits we tried keeping same b -parameter for absorption from all J levels. We constrained the column density to be the same for a given J level and allow it to be different for different J levels. As wavelength scales are not accurate we did allow the redshifts of individual transitions to be different. Best fit is obtained for $b = 4.1 \pm 0.4$ km s⁻¹ with a reduced $\chi^2 = 0.63$. The best fitted column densities from the voigt profile fits are summarized in the last column of Table 1. The best fitted profile overlaid on the observed data are shown in Fig. 2. For consistency check, in this figure we also show the predicted profiles of the blended H₂ lines with the dotted profiles.

The best fitted b parameter is slightly lower and $N(J)$ values are slightly higher than the ones obtained using COG analysis. The column density errors are small in the case of measurements using VPFIT. This is mainly because the quoted errors are only statistical and systematic errors from the continuum placement uncertainties are not included. We also consider voigt profiles fits allowing the b

parameter to be different for different J levels. We find the column densities derived for $J = 0$ and 1 levels are consistent with what we quote in Table 1 even though a lower value of b parameter is preferred. This is the indication that some of these lines are in the damped part of the COG. The value of b is ill-constrained in the case of $J = 3$ as we have only two clean lines used for the fit.

3.2.3 Molecular fraction & Kinetic temperature

Here we estimate physical parameters using H₂ column densities obtained with COG analysis that properly takes care of the continuum placement uncertainties. The total H₂ column density from the COG analysis is $\log N(\text{H}_2) = 18.13 - 18.40$ and the molecular fraction, $-2.11 \leq \log f(\text{H}_2) \leq -1.85^6$. In the Galactic disk $\log f(\text{H}_2)$ is expected to be ≤ -4 for the $N(\text{H I})$ observed in this system (Savage et al. 1977). Such high values of $f(\text{H}_2)$ are not seen for $\log N(\text{H I}) = 20.55$, even in the case of Magellanic clouds (See Fig 8 of Tumlinson et al. 2002). The observed high value of $\log f(\text{H}_2)$ is consistent with what is seen in the high latitude (i.e., $|b| \geq 20^\circ$) clouds in the halo of our Galaxy (see Fig 6 of Gillmon et al. 2006) and also in a couple of high- z DLAs ($z_{\text{abs}} = 2.087$ towards Q 1444+0126 and $z_{\text{abs}} = 2.426$ towards Q 2348-0108 discussed in Ledoux et al. 2003; Noterdaeme et al. 2007). In comparison to the two known H₂ systems at $z \leq 1$, the derived $f(\text{H}_2)$ here is close to what is measured in the $z_{\text{abs}} = 0.56$ sub-DLA towards Q 0107-0232 (Crighton et al. 2013) and an order of magnitude smaller than that measured in the H₂ system at $z_{\text{abs}} = 0.18$ towards B 0120-28 that also shows HD molecules (Oliveira et al. 2014). Equilibrium H₂ abundance is controlled by the formation and the destruction rates. In addition, as H₂ is optically thick in the present case, the effect of shielding becomes very important in establishing the equilibrium H₂ abundance.

It is well known that the H₂ excitation temperature measured using $J = 0$ and $J = 1$ levels (called T_{01}) traces the kinetic temperature of the gas very well when $\log N(\text{H}_2) \geq 15.8$ (see Roy et al. 2006). Using Eq. 3 in Srianand et al. (2005), we estimate $86 \leq T_{01} \leq 270$ K, $78 \leq T_{02} \leq 133$ K and $95 \leq T_{13} \leq 135$ K. This suggests that rotational level populations are consistent with a single excitation temperature in the range 95–133 K. This temperature range is slightly higher than that measured in the Galactic ISM (77 ± 17 K; Savage et al. 1977) and Magellanic clouds (82 ± 21 K; Tumlinson et al. 2002) and consistent with the lower end of what is measured in high- z DLAs (100–300 K; Srianand et al. 2005). Below we discuss the implications of equilibrium abundance of H₂ and the rotational populations using photoionization code CLOUDY.

4 PHOTOIONIZATION MODELS USING CLOUDY

In this section we consider photoionization models constructed using CLOUDY. In order to get an accurate H₂ equilibrium abundance, we use the full J resolved calculations as described in (Shaw et al. 2005) using “atom H₂” command. Given the uncertainties associated with the H I contribution to different phases we do not attempt to model all the absorption species detected in the COS spectrum and focus mainly on H₂, C I, Mg I and C II*. To start with we assume

⁶ The $f(\text{H}_2)$ measured using voigt profile analysis is 0.2 dex higher than that obtained using COG. However, the excitation temperature derived using both the methods are consistent.

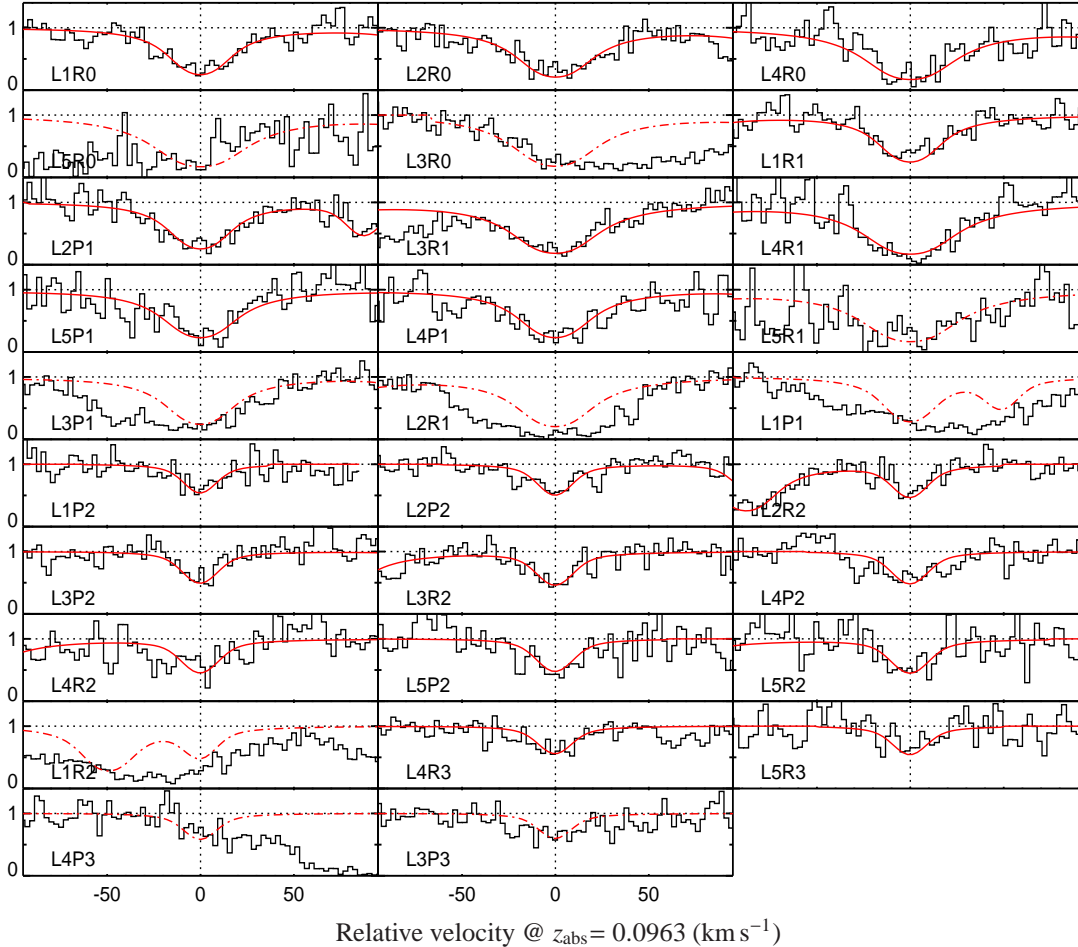


Figure 2. Single component voigt profile fits to H_2 absorption detected in the $z_{\text{abs}} = 0.0963$ DLA towards J1619+3342. The solid smooth profile over-plotted on the observed data is our best fit model. The dashed profiles are the model predictions in cases where the H_2 transition is not used in the fit as they are blended with absorption from other systems.

that all the measured $N(\text{H I})$ is associated to the H_2 component⁷ and consider the absorbing gas to be a single component.

The ionizing radiation considered in our model is a combination of meta-galactic UV background contributed by QSOs and galaxies (Haardt & Madau 1996) and the interstellar radiation field similar to that of the Milky Way (Habing 1968) but scaled by χ_{UV} . The value of χ_{UV} equals to 0 and 1 corresponds to the UV radiation field similar to the meta-galactic UV background and that seen in the Milky Way disk respectively. The absorbing gas is assumed to be a plane-parallel slab with the radiation field illuminating it from one side⁸. The calculation is stopped when $N(\text{H I})$ in the model is equal to the observed value. We assume the metallicity and the dust depletion similar to what is observed for this system and assumed the dust composition to be similar to Milky Way. For most of the models discussed here, we assume cosmic-ray ionization rate, $\log(\Gamma_{CR}) = -17.3$, the default value in `CLOUDY` taken from Williams et al.

⁷ However, it is worth remembering that at high- z it is now recognized that only a small fraction of H I may be associated with the H_2 component (see Srianand et al. 2012).

⁸ We note that considering two sided illumination does not change our results as found by Dutta et al. (2014).

(1998). Later we will explore the effect of using different values of Γ_{CR} .

4.1 Constant temperature models

First we run a set of constant temperature models keeping the gas temperature to be 100 K as inferred from H_2 observations. We find the allowed hydrogen density range (n_H) for a range of χ_{UV} . These are summarised in panel (a) in Fig. 3. In panel (b), we show the predicted values of $N(\text{C I})$ for this allowed density range (shaded region) for each value of χ_{UV} . The dashed horizontal line is the observed 3σ upper limit. It is clear from this figure that model predictions are consistent with the observed $N(\text{C I})$ upper limits, when $\chi_{UV} \geq 0.2$. In this range the H_2 observations are consistent with $n_H \geq 10 \text{ cm}^{-3}$.

It is clear from panel (d) in Fig. 3 that for the range in χ_{UV} and n_H the predicted Mg I column densities are 0.2 dex higher than the observed value. However, it is well known that Mg is depleted by about 0.3 dex even in the halo gas of Milky way (see Table 5, of Welty et al. 1999). The dotted region marks the model prediction when Mg is depleted by 0.3 dex. This is consistent with the observations. Thus C I , Mg I and H_2 observations are consistently repro-

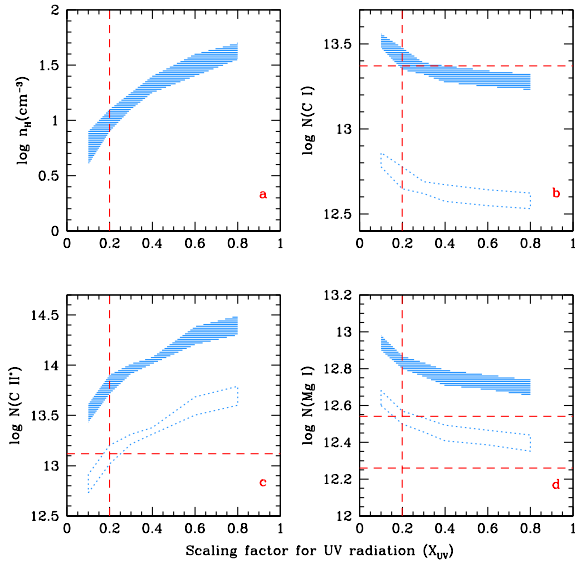


Figure 3. Results of photoionization models using `CLOUDY`. The shaded region in panel (a) gives the allowed density range that reproduces the observed $N(\text{H}_2)$ for a given intensity of the background radiation field (denoted by χ_{UV}). Shaded regions in the remaining panels are the predicted range in the column density of a given species for the density range given in panel (a). Regions marked by dotted lines are the same after taking into account a typical elemental depletion. Horizontal dashed lines are the measurements when there are two lines and upper limit when only one line is present.

duced by the models when a moderate Mg depletion is assumed for $n_H \geq 10 \text{ cm}^{-3}$. We also notice that the model predicted C I column density is also consistent with the measured upper limits.

However, these models have problem reproducing the C II* column density. Panel (c) shows the predicted C II* column density as a function of χ_{UV} for the allowed n_H range given in panel (a). It is clear (from the shaded region) that when the relative abundance of C with respect to other elements is solar our models over predict C II* column density by more than 0.6 dex. The deviation is more for higher values of χ_{UV} . The typical C depletion seen in our Galaxy (i.e., 0.4 dex) alone can not bring the model predicted $N(\text{C II}^*)$ below the upper limit from observations. We need carbon to be underabundant by more than 0.6 dex (see the region covered by the dotted line). Such underabundance of C is not usually seen in DLAs but seen in halo stars with metallicity similar to the present DLA (see Fabbian et al. 2009). One possible way of avoiding the high C depletion is to produce the required amounts of H₂ at lower densities. This we shall explore below.

4.2 Thermal equilibrium models

We run next set of `CLOUDY` simulations allowing the temperature of the gas to be self-consistently computed by `CLOUDY`. We consider $\log(\Gamma_{CR}) = -17.3$ and $0.3 \leq \chi_{UV} \leq 0.6$. We find the observed H₂ column density is reproduced for n_H in the range 20 to 60 cm^{-3} . These models have $\log N(\text{C I})$, and $\log N(\text{Mg I})$ in the range 13.69–13.78 and 13.03–13.10 respectively. These are typically 0.3 dex higher than what we found for constant temperature model above. We notice that this is mainly due to the gas kinetic temperature in the model being very low (i.e., $T = 32 \text{ K}$). Clearly

we need additional heating for the gas to have correct H₂ excitation as well. Such a situation is also encountered while modelling the ISM sightlines using `CLOUDY` (see Shaw et al. 2006, 2008).

Enhancement in the cosmic-ray ionization rate has been suggested as a possible solution to get high temperature in the models. To explore this, we consider a model with $\chi_{UV} \leq 0.6$ and $\log(\Gamma_{CR}) = -15.7$. The observed H₂ abundance is obtained for $1.3 \leq \log n_H [\text{cm}^{-3}] \leq 1.5$. This is similar to what we have in Fig 3. As expected the gas temperature in enhanced and is between 47–60 K. However, C I and Mg I column densities predicted by these models are much higher than the observed values. Thus we do not favor high Γ_{CR} as the reason for high gas temperature.

Next, we considered the stopping column density $N(\text{H I}) = 20.25$ (a factor 2 smaller than the observed value) to mimic the case where only part of the H I column density is associated to the H₂ component or the gas disk is observed at an inclination angle (see Dutta et al. 2014). For simplicity, we considered $\chi_{UV} = 0.5$ and varied $\log(\Gamma_{CR})$ in the range -15.7 to -17.3 . We note that observed constraints from H₂, C I, C II* and Mg I can be satisfied when $1.6 \leq \log(n_H [\text{cm}^{-3}]) \leq 1.8$, $\log(\Gamma_{CR}) = -17.3$ and assume Mg and C are depleted by 0.3 dex and ≥ 0.3 dex respectively. However, like the models discussed above the best fitted models have kinetic temperature of 30 K. The models with high Γ_{CR} gives slightly higher temperature albeit with increased abundances of Mg I and C I.

Low temperatures produced in `CLOUDY` models suggest that additional non-radiative heating processes that are not included in `CLOUDY` may be playing a crucial role in heating the gas. Indeed numerical simulations of SNe driven interstellar medium use energy from the SNe in various forms to get the gas temperature (see for example, Korpi et al. 1999; Gazol et al. 2001; Mac Low et al. 2005; Joung et al. 2009). If such a mechanical injection of energy is available in the present system also then the excess temperature noted can be explained.

4.3 Models with enhanced H₂ formation rate:

From the discussions presented above, it appears that the best solution to the lack of C I and C II* absorption and high kinetic temperature is to produce the required amounts of H₂ at lower densities. One of the possibilities is to increase the H₂ formation rates on top of the dust grains. Note, it is a general procedure to use the H₂ formation rate (i.e., $3 \times 10^{-17} \text{ cm}^3 \text{ s}^{-1}$) inferred by Jura (1974) in the analytic calculations to model systems with H₂ detections. However, there are indications that these mean H₂ formation rate may not be sufficient to explain properties of Photo-Dissociation Regions (PDR) with low to moderate excitation and enhanced formation rate may be needed (see Habart et al. 2011; Le Bourlot et al. 2012). To explore this, we run `CLOUDY` with an enhanced H₂ formation rate by a factor 2 to that of Jura (1974). We note that the observed constraints can be explained by a model with $\chi_{UV} \sim 0.2$, $0.6 \leq \log(n_H [\text{cm}^{-3}]) \leq 0.8$. However, these models still have gas kinetic temperature ($\sim 50 \text{ K}$) a factor 2 smaller than what we infer from the data. Le Bourlot et al. (2012) have suggested that the grain physics included in their calculations that enhances the H₂ formation rate can also produce formation heating. As these dust processes are not yet incorporated in `CLOUDY` we could not check whether the additional formation heating can enhance the temperature to the observed value.

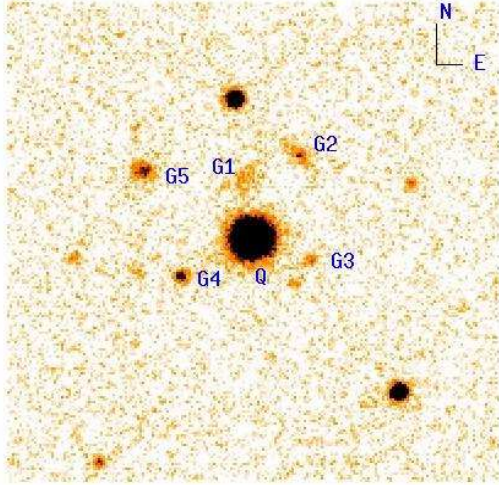


Figure 4. R-band image covering $1' \times 1'$ centered around the QSO. The QSO and 5 galaxies close to the QSO in the angular scale are marked. Only galaxy G1 has the photometric redshift consistent with the z_{abs} of the DLA. We consider this as the candidate host galaxy of the DLA. The seeing measured in this image is close to 1.4 arc sec.

5 GALAXY CANDIDATES

We do not detect any line emission from the intervening galaxy in the SDSS fiber spectrum of the QSOs (for example, as seen in Noterdaeme et al. 2010b). Using the measured signal-to-noise and a line width of 300 km s^{-1} we find a 3σ upper limit on $H\alpha$ luminosity to be 1.63×10^{34} watts. The upper limit for the $H\alpha$ flux is consistent with a surface star formation rate of $\leq 2.3 \times 10^{-2} M_{\odot} \text{ yr}^{-1} \text{ kpc}^{-2}$ assuming the absorbing galaxy fills the SDSS fibre. This limit is not stringent enough and allows for star formation similar to what is measured in the case of low- z 21-cm absorbers that show emission lines in the SDSS fibre spectra (see Table 3 of Gupta et al. 2013). In these cases one sees low surface brightness star forming galaxies whose disk is pierced by the QSO sight line. Alternatively it is possible that the absorbing gas is at a high impact parameter to the host galaxy as usually identified in the past for low- z DLAs (for e.g. Rao et al. 2003).

In our IGO R and V band images we identify 5 galaxies within 30 arc sec to the QSOs as shown in Fig. 4. Among them four galaxies (excluding G1) have photometric redshifts (based on our’s and available SDSS photometry) greater than 0.3. The galaxy G1 has consistent photometric redshift to the absorber albeit with large errors (i.e., $z_p = 0.10 \pm 0.08$). In the absence of spectroscopic data we consider this as a possible candidate DLA galaxy for further discussions. This galaxy is at a projected separation of 8 arcsec from the QSO sight line. This corresponds to an impact parameter of 14.2 kpc for the assumed cosmology (i.e., Flat universe with $\Omega_{\Lambda} = 0.73$ and $\Omega_m = 0.27$ and $H_0 = 71 \text{ km/s/Mpc}$). The R and V band magnitudes of this galaxy are 21.50 and 20.85 mag respectively. Thus the identified galaxy is a sub- L_* galaxy. The inferred impact parameter is less than the median impact parameter for low- z DLAs found by Rao et al. (2003) and similar to what is found for $z \sim 0.1$ Mg II absorber (Kacprzak et al. 2011).

6 SUMMARY AND DISCUSSIONS

We report the detection of H_2 in a DLA at $z_{\text{abs}} = 0.0963$ toward J1619+3342. The inferred molecular fraction ($-2.11 \leq \log f(\text{H}_2) \leq -1.85$) for the observed $\log N(\text{H I}) = 20.55 \pm 0.10$ is much higher than what has been seen in the Milky Way and in Magellanic clouds but consistent with what is measured in high latitude gas in the Milky way halo (Gillmon et al. 2006). In this case it was suggested that the enhanced H_2 formation rate in the dense compressed gas may be the reason for the enhanced H_2 even at low $N(\text{H I})$. This is also similar to what has been observed in the $z_{\text{abs}} = 0.56$ sub-DLA towards Q 0107-0232 (Crighton et al. 2013). Using the rotational excitation of H_2 we infer the kinetic temperature of the gas to be in the range 95 to 133 K. This is slightly higher than the typical temperature measured in the Galactic ISM. But consistent with what is seen in high- z DLAs. In the absence of fine-structure lines of C I and C II stringent density measurements are not possible.

The observed metallicity is $[\text{S}/\text{H}] = -0.62 \pm 0.13$ similar to what is seen in the SMC. The observed depletion $[\text{Fe}/\text{S}] = -1.00 \pm 0.17$ is much less than what is seen in the Milky Way. We find $N(\text{Ti II})/N(\text{Ca II}) \sim 0.3$ consistent with what is measured in the Milky Way and larger than what is measured in Magellanic clouds. We also find no relative depletion between Fe II and Ti II. This is consistent with the absence of strong radiation field effects. In summary, the inferred metallicity is similar to the mean value measured in SMC sight lines with the dust depletion intermediate between lower Milky Way halo gas and LMC sight lines. If the strong correlation seen between the average line of sight density and Ti depletion is applicable in the present case also then we can conclude that the average density in the present DLA may be lower than that typically seen in the Milky Way disk.

Unlike most of the high- z DLAs, we do not detect C I or C II*. Based on the $N(\text{C II}^*)$ upper limits we estimate the gas cooling rate, $\log l_c \leq -27.03 \text{ erg s}^{-1}$ per hydrogen atom. Therefore, this system belongs to the “low-cool” population of DLAs defined by Wolfe et al. (2008). If C is not depleted then this also implies the average density may be less than what is typically seen in diffuse molecular gas in the Galactic ISM.

We consider wide range of photoionization model to understand the physical conditions in the H_2 components. When we consider all H I column density measured along the line of sight is associated with the H_2 components we find constraints for C I, C II* and Mg I can be explained only when a C is depleted by more than 0.6 dex as seen in the low metallicity star in the Milky Way. These models require hydrogen density in the range, $1.0 \leq \log(n_{\text{H}}) \leq 1.5$. Alternatively the observed constraints can be explained by assuming only part of the observed $N(\text{H I})$ is associated to the H_2 component or the H_2 formation rate on the dust grain is at least a factor 2 higher than the typical value used in the Milky Way ISM models. In the first case the required hydrogen density is slightly higher than that quoted above. In the second case the required density range is $0.60 \leq \log(n_{\text{H}}) \leq 0.8$. However, all the photoionization models produce gas temperature typically a factor 2 less than the observed value. We conjecture that additional heating like SNe heating seen in the hydrodynamical ISM simulations may also be important in this system.

We do not find any signatures of starformation activities along the line of sight based on the lack of emission line detection in the QSO fiber spectra. We identify a sub- L_* galaxy at a impact parameter of 14.2 kpc as a possible candidate for the DLA galaxy. This is consistent with the H_2 gas either associated with a very low luminosity galaxy along the line of sight or in the halo of the iden-

tified galaxy. Detailed spectroscopic study of faint galaxies around this QSO is important to further understand this H₂ system without speculating too much.

7 ACKNOWLEDGEMENTS

We thank the IGO staffs for their help during observations.

REFERENCES

- Akerman C. J., Carigi L., Nissen P. E., Pettini M., Asplund M., 2004, *A&A*, 414, 931
- Altay G., Theuns T., Schaye J., Crighton N. H. M., Dalla Vecchia C., 2011, *ApJ*, 737, L37
- Balashev S. A., Petitjean P., Ivanchik A. V., Ledoux C., Srianand R., Noterdaeme P., Varshalovich D. A., 2011, *MNRAS*, 418, 357
- Battisti A. J., Meiring J. D., Tripp T. M., Prochaska J. X., Werk J. K., Jenkins E. B., Lehner N., Tumlinson J., Thom C., 2012, *ApJ*, 744, 93
- Bouché N., Murphy M. T., Kacprzak G. G., Péroux C., Contini T., Martin C. L., Dessauges-Zavadsky M., 2013, *Science*, 341, 50
- Burbidge E. M., Beaver E. A., Cohen R. D., Junkkarinen V. T., Lyons R. W., 1996, *AJ*, 112, 2533
- Cox N. L. J., Cordiner M. A., Cami J., Foing B. H., Sarre P. J., Kaper L., Ehrenfreund P., 2006, *A&A*, 447, 991
- Cox N. L. J., Cordiner M. A., Ehrenfreund P., Kaper L., Sarre P. J., Foing B. H., Spaans M., Cami J., Sofia U. J., Clayton G. C., Gordon K. D., Salama F., 2007, *A&A*, 470, 941
- Crighton N. H. M., Bechtold J., Carswell R. F., Davé R., Foltz C. B., Jannuzi B. T., Morris S. L., O'Meara J. M., Prochaska J. X., Schaye J., Tejos N., 2013, *MNRAS*, 433, 178
- Danforth C. W., Keeney B. A., Stocke J. T., Shull J. M., Yao Y., 2010, *ApJ*, 720, 976
- Dutta R., Srianand R., Rahmani H., Petitjean P., Noterdaeme P., Ledoux C., 2014, *ArXiv*: 1402.2975
- Fabbian D., Nissen P. E., Asplund M., Pettini M., Akerman C., 2009, *A&A*, 500, 1143
- Fox A. J., Ledoux C., Petitjean P., Srianand R., 2007, *A&A*, 473, 791
- Fynbo J. P. U., Geier S. J., Christensen L., Gallazzi A., Krogager J.-K., Krühler T., Ledoux C., Maund J. R., Møller P., Noterdaeme P., Rivera-Thorsen T., Vestergaard M., 2013, *MNRAS*, 436, 361
- Gazol A., Vázquez-Semadeni E., Sánchez-Salcedo F. J., Scalo J., 2001, *ApJ*, 557, L121
- Ghavamian P., Aloisi A., Lennon D., Hartig G., Kriss G. A., Oliveira C., Massa D., Keyes T., Proffitt C., Delker T., Osterman S., 2009, Preliminary Characterization of the Post-Launch Line Spread Function of COS. Tech. rep.
- Gillmon K., Shull J. M., Tumlinson J., Danforth C., 2006, *ApJ*, 636, 891
- Gupta N., Srianand R., Noterdaeme P., Petitjean P., Muzahid S., 2013, *A&A*, 558, A84
- Haardt F., Madau P., 1996, *ApJ*, 461, 20
- Habart E., Abergel A., Boulanger F., Joblin C., Verstraete L., Compiègne M., Pineau Des Forêts G., Le Bourlot J., 2011, *A&A*, 527, A122
- Habing H. J., 1968, *Bull. Astron. Inst. Netherlands*, 19, 421
- Joung M. R., Mac Low M.-M., Bryan G. L., 2009, *ApJ*, 704, 137
- Jura M., 1974, *ApJ*, 191, 375
- Kacprzak G. G., Churchill C. W., Barton E. J., Cooke J., 2011, *ApJ*, 733, 105
- Kashikawa N., Misawa T., Minowa Y., Okoshi K., Hattori T., Toshikawa J., Ishikawa S., Onoue M., 2014, *ApJ*, 780, 116
- Korpi M. J., Brandenburg A., Shukurov A., Tuominen I., Nordlund Å., 1999, *ApJ*, 514, L99
- Kriss G. A., 2011, Improved Medium Resolution Line Spread Functions for COS FUV Spectra. Tech. rep.
- Le Bourlot J., Le Petit F., Pinto C., Roueff E., Roy F., 2012, *A&A*, 541, A76
- Le Brun V., Bergeron J., Boissé P., Deharveng J. M., 1997, *A&A*, 321, 733
- Ledoux C., Petitjean P., Srianand R., 2003, *MNRAS*, 346, 209
- Lehner N., Wakker B. P., Savage B. D., 2004, *ApJ*, 615, 767
- Mac Low M.-M., Balsara D. S., Kim J., de Avillez M. A., 2005, *ApJ*, 626, 864
- Meiring J. D., Lauroesch J. T., Haberzettl L., Kulkarni V. P., Péroux C., Khare P., York D. G., 2011, *MNRAS*, 410, 2516
- Meiring J. D., Tripp T. M., Werk J. K., Howk J. C., Jenkins E. B., Prochaska J. X., Lehner N., Sembach K. R., 2013, *ApJ*, 767, 49
- Noterdaeme P., Ledoux C., Petitjean P., Srianand R., 2008a, *A&A*, 481, 327
- Noterdaeme P., Ledoux C., Srianand R., Petitjean P., Lopez S., 2009a, *A&A*, 503, 765
- Noterdaeme P., Petitjean P., Carithers W. C., Pâris I., Font-Ribera A., Bailey S., Aubourg E., Bizyaev D., Ebelke G., Finley H., Ge J., Malanushenko E., Malanushenko V., Miralda-Escudé J., Myers A. D., Oravetz D., Pan K., Pieri M. M., Ross N. P., Schneider D. P., Simmons A., York D. G., 2012, *A&A*, 547, L1
- Noterdaeme P., Petitjean P., Ledoux C., López S., Srianand R., Vergani S. D., 2010a, *A&A*, 523, A80
- Noterdaeme P., Petitjean P., Ledoux C., Srianand R., 2009b, *A&A*, 505, 1087
- Noterdaeme P., Petitjean P., Ledoux C., Srianand R., Ivanchik A., 2008b, *A&A*, 491, 397
- Noterdaeme P., Petitjean P., Srianand R., Ledoux C., Le Petit F., 2007, *A&A*, 469, 425
- Noterdaeme P., Petitjean P., Srianand R., Ledoux C., López S., 2011, *A&A*, 526, L7
- Noterdaeme P., Srianand R., Mohan V., 2010b, *MNRAS*, 403, 906
- Oliveira C. M., Sembach K. R., Tumlinson J., O'Meara J., Thom C., 2014, *ApJ*, 783, 22
- Pequignot D., Aldrovandi S. M. V., 1986, *A&A*, 161, 169
- Petitjean P., Ledoux C., Noterdaeme P., Srianand R., 2006, *A&A*, 456, L9
- Pontzen A., Governato F., Pettini M., Booth C. M., Stinson G., Wadsley J., Brooks A., Quinn T., Haehnelt M., 2008, *MNRAS*, 390, 1349
- Prochaska J. X., Herbert-Fort S., Wolfe A. M., 2005, *ApJ*, 635, 123
- Rao S. M., Nestor D. B., Turnshek D. A., Lane W. M., Monier E. M., Bergeron J., 2003, *ApJ*, 595, 94
- Rao S. M., Turnshek D. A., Nestor D. B., 2006, *ApJ*, 636, 610
- Roy N., Chengalur J. N., Srianand R., 2006, *MNRAS*, 365, L1
- Savage B. D., Bohlin R. C., Drake J. F., Budich W., 1977, *ApJ*, 216, 291
- Savage B. D., Narayanan A., Lehner N., Wakker B. P., 2011, *ApJ*, 731, 14
- Shaw G., Ferland G. J., Abel N. P., Stancil P. C., van Hoof P. A. M., 2005, *ApJ*, 624, 794
- Shaw G., Ferland G. J., Srianand R., Abel N. P., 2006, *ApJ*, 639, 941

- Shaw G., Ferland G. J., Srianand R., Abel N. P., van Hoof P. A. M., Stancil P. C., 2008, *ApJ*, 675, 405
- Sofia U. J., Parvathi V. S., Babu B. R. S., Murthy J., 2011, *AJ*, 141, 22
- Srianand R., Gupta N., Petitjean P., Noterdaeme P., Ledoux C., Salter C. J., Saikia D. J., 2012, *MNRAS*, 421, 651
- Srianand R., Noterdaeme P., Ledoux C., Petitjean P., 2008, *A&A*, 482, L39
- Srianand R., Petitjean P., Ledoux C., Ferland G., Shaw G., 2005, *MNRAS*, 362, 549
- Tumlinson J., Shull J. M., Rachford B. L., Browning M. K., Snow T. P., Fullerton A. W., Jenkins E. B., Savage B. D., Crowther P. A., Moos H. W., Sembach K. R., Sonneborn G., York D. G., 2002, *ApJ*, 566, 857
- Varshalovich D. A., Ivanchik A. V., Petitjean P., Srianand R., Ledoux C., 2001, *Astronomy Letters*, 27, 683
- Vladilo G., Centurión M., D'Odorico V., Péroux C., 2003, *A&A*, 402, 487
- Welty D. E., Crowther P. A., 2010, *MNRAS*, 404, 1321
- Welty D. E., Hobbs L. M., Lauroesch J. T., Morton D. C., Spitzer L., York D. G., 1999, *ApJS*, 124, 465
- Welty D. E., Hobbs L. M., Morton D. C., 2003, *ApJS*, 147, 61
- Williams J. P., Bergin E. A., Caselli P., Myers P. C., Plume R., 1998, *ApJ*, 503, 689
- Wolfe A. M., Gawiser E., Prochaska J. X., 2003, *ApJ*, 593, 235
- , 2005, *ARA&A*, 43, 861
- Wolfe A. M., Prochaska J. X., Jorgenson R. A., Rafelski M., 2008, *ApJ*, 681, 881